Electronic Supplementary Material (ESI) for Nanoscale Advances.

Supplementary Information for Growth pathways of Cu shells on Au and AuCu seeds: interdiffusion, shape transformations, strained shells and patchy surfaces

El Yakout El Koraychy and Riccardo Ferrando*

Dipartimento di Fisica, Università di Genova, Via Dodecaneso 33, 16146 Genova, Italia

E-mail: ferrando@fisica.unige.it

Stability of initial seeds

In Figure S1 we present the excess energy E_{exc} per atom of truncated octahedron and icosahedron initial seeds for some compositions together with the number of Cu atoms in the surface of each structure. This quantity has been calculated to determine the lowest-energy composition within the truncated octahedron of N=201 atoms and icosahedron of N=309 atoms structural motifs. E_{exc} is defined as:

$$E_{exc}(m,n) = E(m,n) - \frac{m}{N}E(N,0) - \frac{n}{N}E(0,N), \tag{1}$$

where $E(m,n)$ is the binding energy of the Au_mCu_n cluster. $E(N,0)$ and $E(0,N)$ represent the energy of pure Au and Cu at fixed geometry. For truncated octahedral structure, our chemical ordering searches shows that the lowest excess energy is obtained for composition $Au_{107}Cu_{94}$, corresponding to m/N=0.532 which is closer to 50%-50%. Whereas, for the icosa-

hedral shape, we note that the minimum shift to the composition m/N=0.563, corresponding to $Au_{174}Cu_{135}$.

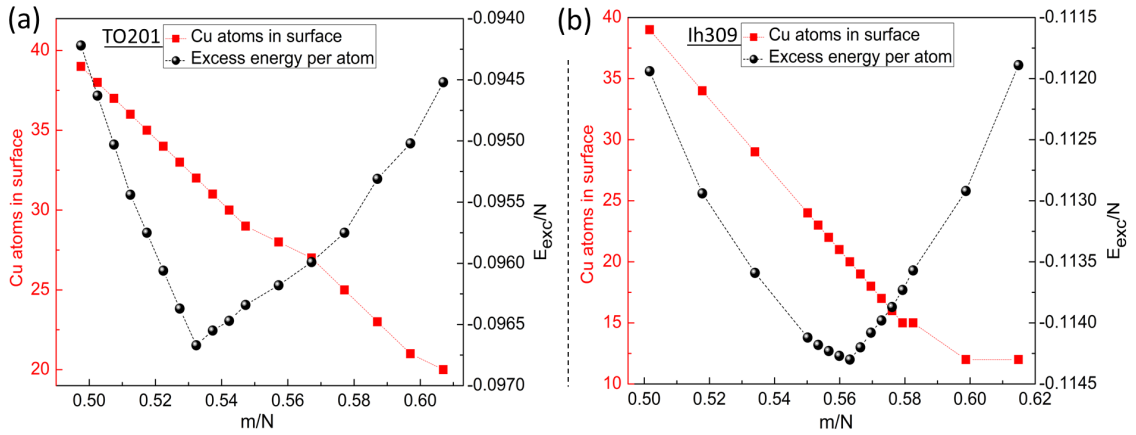

Figure S 1: Excess energy per atom (in eV) for the Au_mCu_m (a) truncated octahedron of m + n = N = 201 atoms and (b) icosahedron of 309 atoms.

Growth on Ih preformed seeds

In Figure S2, we give the plot of radial distribution function of Au and Cu atoms for the final shapes obtained from the growth on Ih with pure and intermixed compositions. Depending on composition of the starting seed and growth temperature, different types of chemical ordering are obtained.

Figure S3 figure out the quantitative analysis of chemical ordering within the growing nanoparticle during Cu deposition on Ih seeds. First row shows (a) number of nearest neighbour mixed Au-Cu bonds, (b) number of Au atoms on the surface and (c) ratio of gyration radius of Au atoms during the Cu deposition on pure Ih seed. Whereas, in second row we represent the same quantities for the growth on Ih mixed seed.

In Figure S2 we give the mechanisms observed during the growth of Ih shape with intermixed chemical ordering from pure Ih seed at temperature 500 K : (a) surface reconstruction, (b) formation of vacancies in the core of the cluster, (c) and (d) ejection of gold atoms to the surface and their incorporation, respectively.

In Figure S5 the growth pathway of icosahedra at $T = 400$ K and deposition rate of 0.1 atom/ns is shown. The simulation starts from an icosahedron of 309 atoms with AuCu mixed composition.

In Figure S6, we represent the interdiffusion of single Cu atom in Au icosahedron of size 309 atoms. The results are given from simulations at temperatures 300 and 500 K. As anticipated, the diffusion of Cu atom towards the inner sites of Au icosahedron depends on temperature. At 300 K, Cu interdiffusion is limited to the subsurface sites. Whereas, at 500 K Cu atom can reach the subsubsurface shell. This indicates a strong interdiffusion during the growth at 500 K and a weak interdiffusion during the growth at 300 K.

In Figure S7, we report the evolution of Δ for Cu atoms on AuCu icosahedron structure. The parameter was computed for each time step from the equation:

$$\Delta = \frac{E_{tot} - N_{Au}E_{coh}^{Au} - N_{Cu}E_{coh}^{Cu}}{N}, \tag{2}$$

E_{tot} is the potential energy of the cluster, E_{coh}^{Au} and E_{coh}^{Cu} are the cohesive energies per atom in the bulk crystal, N_{Au} and N_{Cu} are respectively the number of Au and Cu atoms in the cluster. N represents the cluster size. The aim of this investigation is to understand the stable stacking of Cu atoms on AuCu icosahedral seed. To this end, we consider two different stacking of Cu cap: Mackay and anti-Mackay. For each case, the Cu cap contains 51 atoms and the icosahedron contains 309 atoms with 174 Au atoms and 135 Cu atoms. By simulating at constant T and N for 10 ns, we found that neither Mackay nor anti-Mackay stacking is favourable for Cu atoms on AuCu icosahedron. This means that ideal fcc or hcp stacking of Cu atoms on AuCu icosahedron is not possible due to the lattice mismatch between AuCu seed and Cu growing shell.

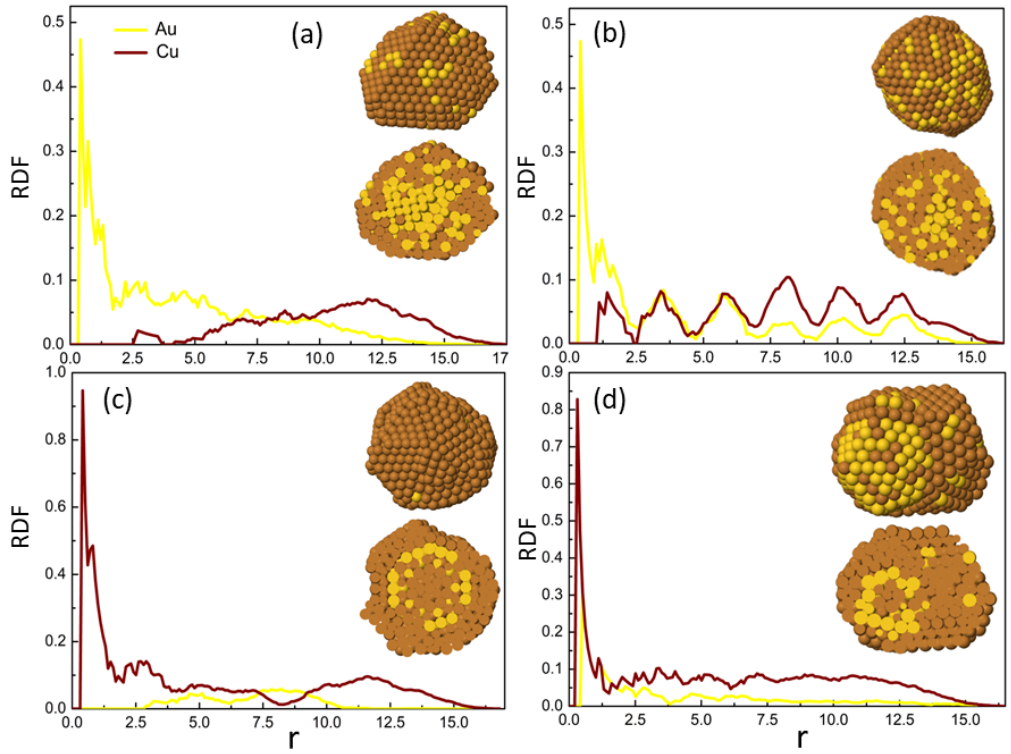

Figure S 2: Radial distribution function of Au and Cu atoms for the final structures obtained during the growth on Ih seeds at temperatures 300 and 500 K. Upper row shows the results for nanoparticles growing from pure Ih seed. Lower row represents the radial distribution within nanoparticles growing from mixed Ih seed. For each column the results are shown for simulation at (a),(c) 300 K and (b),(d) 500 K.

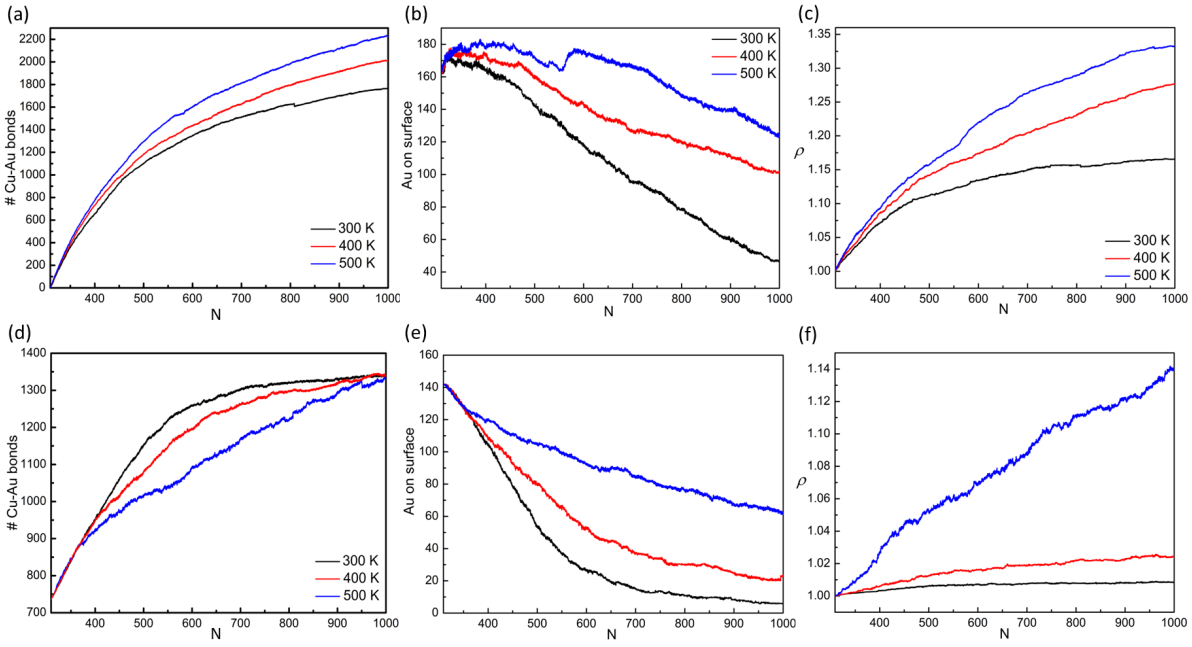

Figure S 3: Number of mixed nearest-neighbour bonds, Au on surface and gyration radius during Cu deposition on Ih seeds. Upper row shows the results for pure starting seed. Lower row represents the ones when depositing Cu atoms on mixed seed.

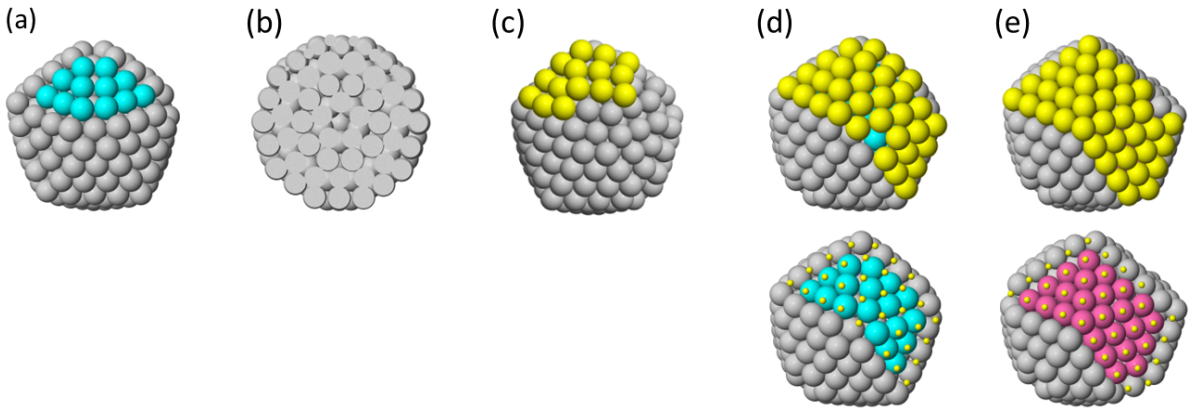

Figure S 4: Different mechanisms generated during the growth of intermixed icosahedral nanoparticle presented in Fig. 6 in the main text. (a) Surface reconstraction; (b) central vacancy; (c) ejected gold atoms; (d) incorporation of ejected gold atoms into the surface and reconstruction of atoms beneath; (e) atoms rearrangement. Gray spheres represent atoms in the initial icosahedral positions. Cyan spheres show atoms in faulted positions. Yellow spheres represent ejected and incorporated gold atoms into the surface. Pink spheres show atoms beneath in the correct positions of the Mackay icosahedral lattice.

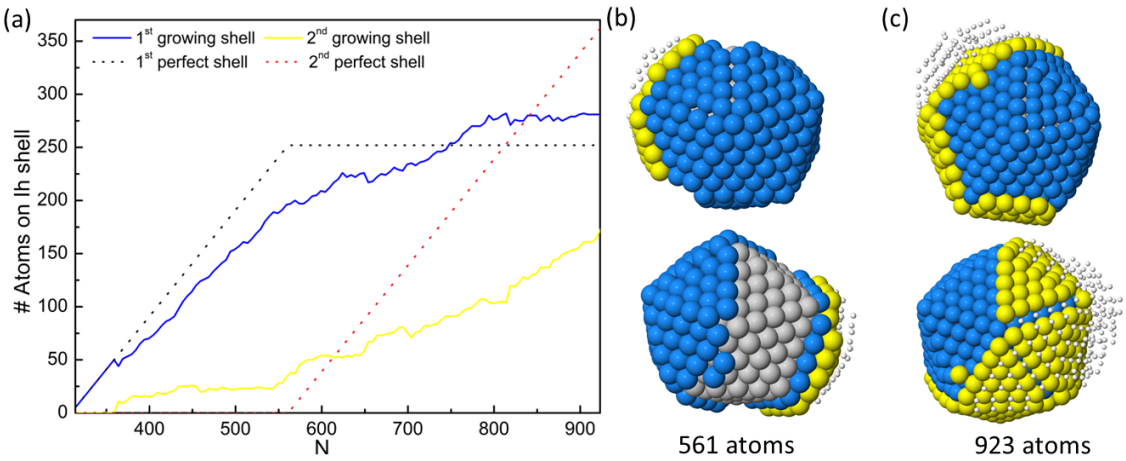

Figure S 5: (a) Evolution of atoms number on the Ih shells during the growth process on Ih mixed seed. Surface view of nanoparticle at two different magic sizes (b) 561 atoms and (c) 923 atoms. For each size the nanoparticle is shown from two different sides. All results are taken from simulations at 400 K and deposition rate of 1 atom each 10 ns.

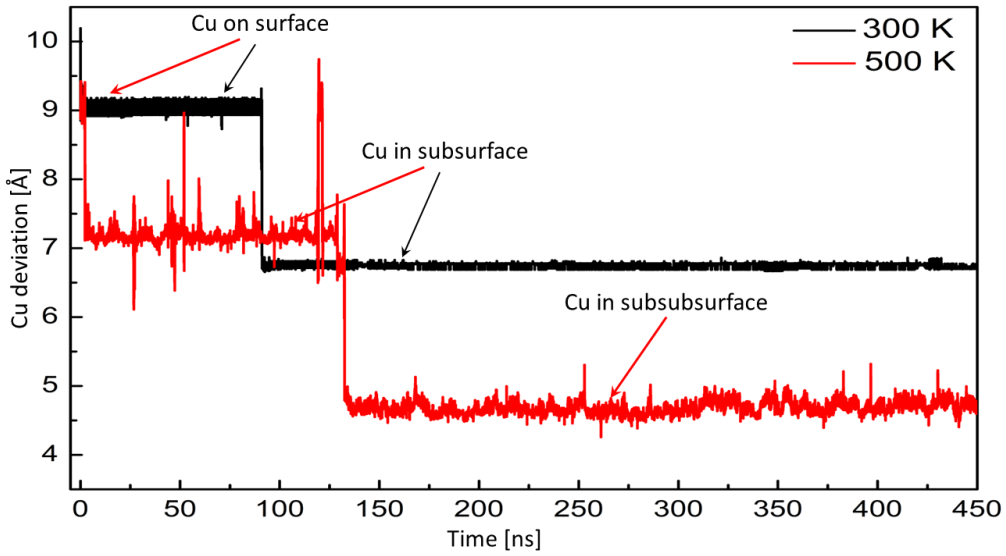

Figure S 6: Interdiffusion of single Cu atom throughout Au icosahedron of size 309 atoms. The results are taken from simulation at constant temperatures (300 and 500 K) for duration of 450 ns.

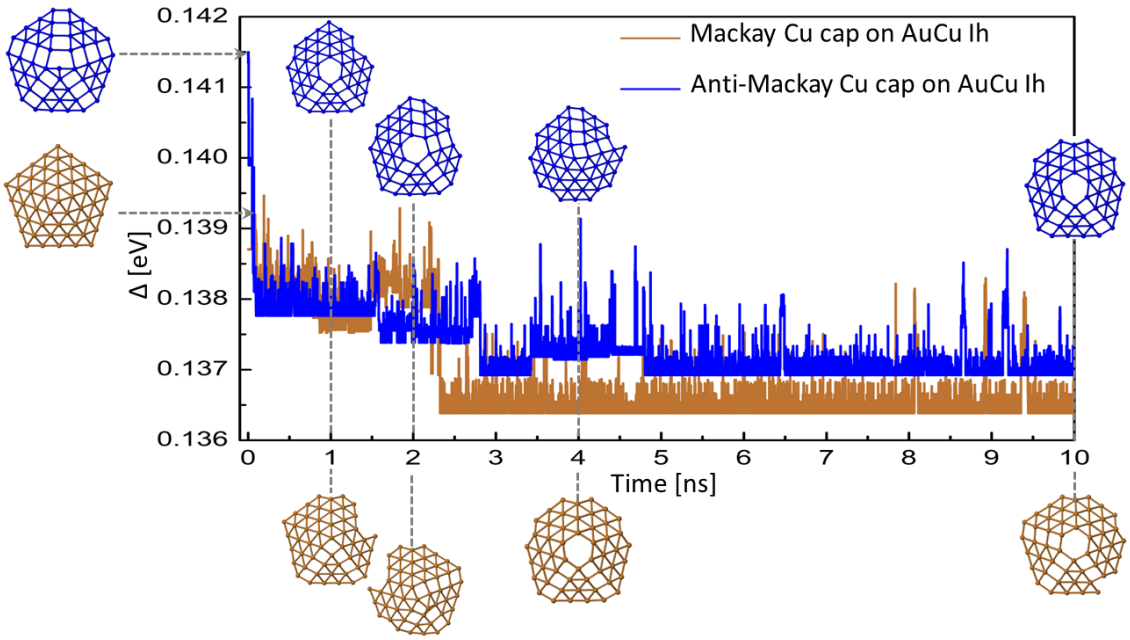

Figure S 7: Δ values of Cu cap on icosahedron for each time step. The results are taken from simulations at temperature 500 K for duration of 10 ns. Brown plot shows the evolution of Δ when Cu atoms in Mackay stacking and blue plot when they are in anti-Mackay stacking. Insets show the lattice of Cu cap at different steps for each starting configuration.

Growth on TO and Dh seeds

Figure S8 gives the radial distribution function of Au and Cu atoms within the final nanoparticles obtained from the growth on TO and Dh with pure and mixed compositions at temperature 300 K. All plots show the core@shell chemical ordering, where the core is made of pure Au or intermed AuCu and the shell is made of Cu.

Figure S9 shows the number of Au-Cu bonds when depositing Cu atoms on TO and Dh seeds. For each shape of the starting seed, the results are given both for pure and mixed at three different temperatures. Plots (a) and (b) represent the evolution of Au-Cu bonds number when starting from pure TO and Dh seeds, respectively. However, the results for the growth on mixed composition are presented in plots (c) and (d).

In Figure S9, we present the number of Au atoms on the surface of the growing nanoparticles for all considered seeds and temperatures. In all results, we find that the number of Au atoms on the surface decreases as the nanoparticle size increases. The comparison

between the results of different starting seeds show that the tendency of Au segregation is found higher when growing on pure Au icosahedral seed at higher temperature and almost negligible when growing on mixed AuCu decahedral seed at lower temperature.

In Figure S11, we present the gyration radii of Au atoms within the nanoparticles during the deposition of Cu atoms on TO and Dh seeds. In all cases, the gyration radius of Au atoms increases with nanoparticle size. However, the results show that the diffusion of Au atoms within the nanoparticle depends on temperature. As anticipated, it is somewhat activated at low temperature and strong at high temperature. For pure seeds, the gyration radius of Au atoms is qualitatively similar for the different shape of the starting seeds and in same order of magnitude. For mixed seeds, a different behavior is observed. For both initial seeds, the evolution of gyration radius exhibits the same behaviour. In the first stage the gyration radius increases with the nanoparticles number, after the deposition of some tens of atoms, the gyration radius remains constant until the end of the simulations.

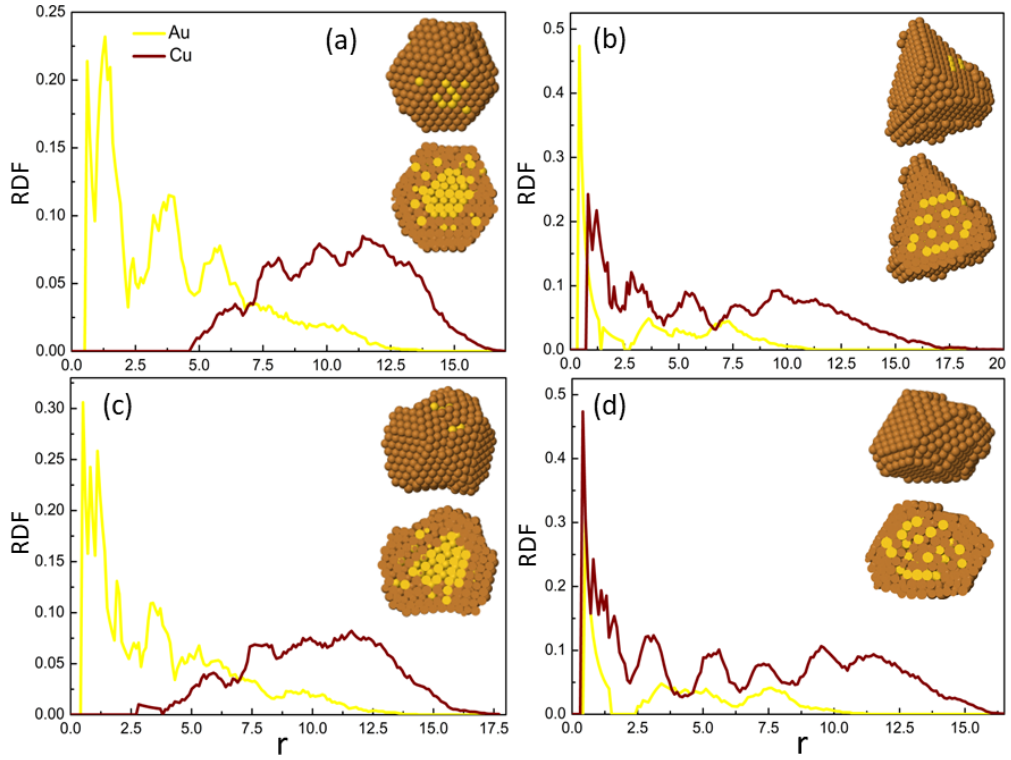

Figure S 8: Radial distribution functions of Au and Cu atoms for the final structures obtained during the growth on TO and Dh seeds at temperature T =300 K. The upper row shows the results for nanoparticles growing from TO seeds. Yellow and brown lines refer to Au and Cu atoms, respectively. The lower row represents the radial distribution function of nanoparticles growing from Dh seeds. For both columns, the results are shown for (a),(c) pure Au seeds and (b),(d) mixed AuCu seeds.

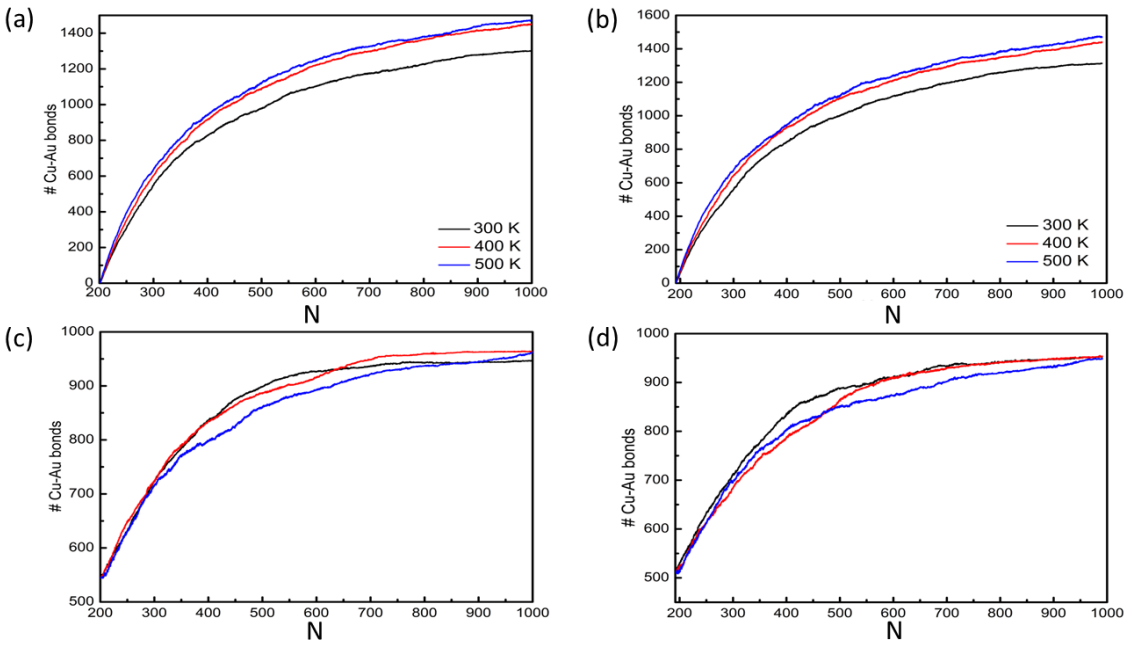

Figure S 9: Evolution of mixed bonds number during Cu deposition on TO and Dh seeds at three different temperatures. (a) and (b) show the results for pure seeds. (c) and (d) represent those for mixed seeds.

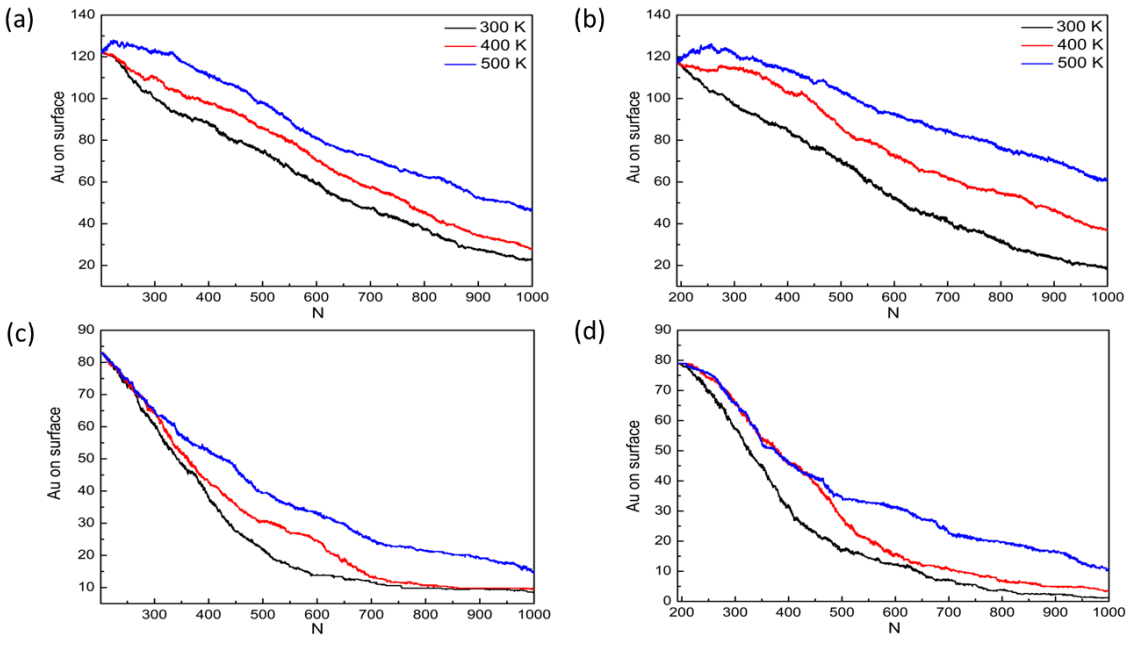

Figure S 10: Number of Au atoms on the surface of nanoparticles during Cu deposition on TO and Dh seeds. Upper row shows the results for Cu on pure seeds and lower row corresponds those for Cu on mixed seeds. Each column represents the data for Au atoms in different shapes of the starting seed. From left to right: Au in truncated octahedron, Au in decahedron and Au in icosahedron. The data are averaged over the five independent simulations.

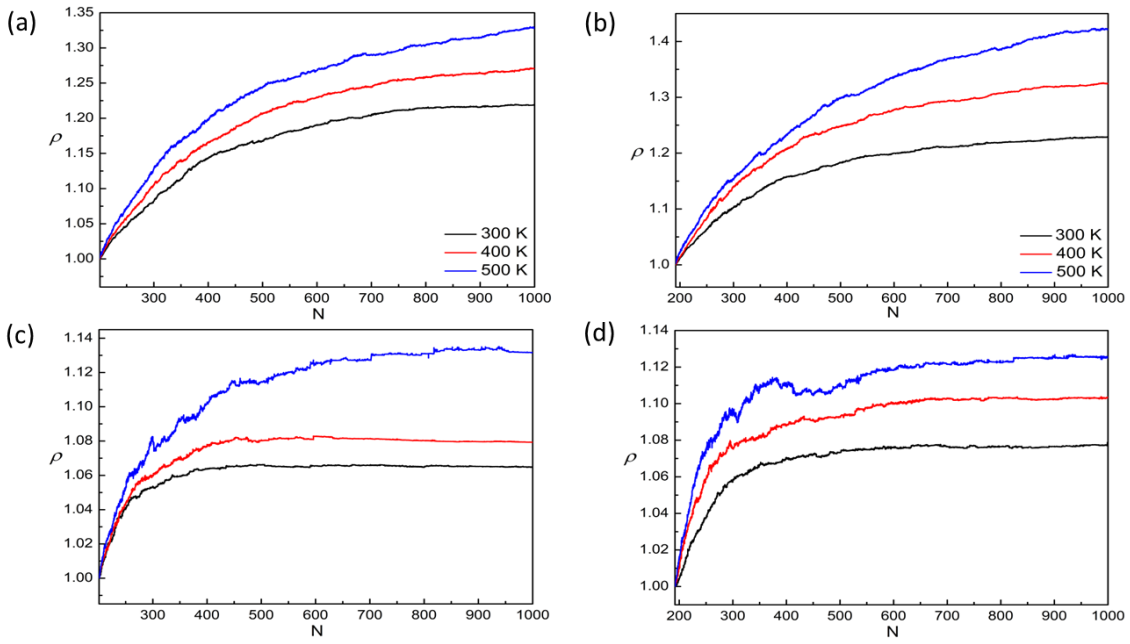

Figure S 11: Evolution of gyration radius during the growth process on TO and Dh at different temperatures. Each plot corresponds to each considered composition of the starting seed. The results are averaged over all simulations.